Materials Horizons

COMMUNICATION

Cite this: *Mater. Horiz.*, 2020, 7, 2719

Received 11th June 2020,
Accepted 27th July 2020

DOI: 10.1039/d0mh00955e

rsc.li/materials-horizons

Enhanced charge separation and photocatalytic hydrogen evolution in carbonized-polymer-dot-coupled lead halide perovskites†

Yue Zhao,‡[a] Qingsen Zeng,‡[a] Yue Yu,[a] Tanglue Feng,[a] Yajie Zhao,[b] Zidong Wang,[a] Yi Li,[b] Chongming Liu,[a] Junjun Liu,[a] Haotong Wei,[a] Shoujun Zhu,[a] Zhenhui Kang,*[b] Hao Zhang[a] and Bai Yang*[a]

Metal halide perovskites are promising candidates as photocatalysts due to their uniquely outstanding photophysical properties; however, the catalytic efficiency is limited by severe charge recombination. Herein, we show that carbonized polymer dots (CPDs) can act as an efficient charge modulator to stabilize photo-generated carriers in methylamine lead triiodide ($MAPbI_3$) perovskites through ultra-fast hole transfer, and thus increase the rate of visible light-driven photocatalytic HI splitting 35-fold. The optimized CPD/$MAPbI_3$/Pt hybrid photocatalytic system exhibits an impressive H_2 evolution rate of 11 497 μmol h^{-1} g^{-1}, a solar-to-hydrogen conversion efficiency of 2.15%, and an apparent quantum yield of 53.6% at 420 nm, which are among the highest values for metal halide perovskite photocatalysts. Moreover, the presented strategy of hole extraction *via* CPDs can be universally applied to improve the performance of previous electron-manipulated $MAPbI_3$-based photocatalytic systems. The easy-to-prepare and bandedge-tunable CPDs with excellent charge-transfer ability may bring new insights in developing high-performance perovskite photocatalysts.

New concepts

Metal halide perovskite (MHP) photocatalysts have caught increasing attention because of their high intrinsic absorption coefficients and low surface recombination velocities. However, the performance is limited by the inefficient charge separation and utilization. In this work, we provide a completely new and highly efficient pathway to enhance charge separation in MHP through coupling with carbonized polymer dots (CPDs). CPDs can stabilize photo-generated carriers in methylamine lead triiodide ($MAPbI_3$) perovskites through ultra-fast hole transfer. The long-lived photoeletrons in CPD-coupled $MAPbI_3$ facilitate photocatalytic reduction reaction and thus increase the rate of visible light-driven HI splitting 35-fold. An H_2 evolution rate of 11 497 μmol h^{-1} g^{-1} and solar-to-hydrogen conversion efficiency of 2.15% are achieved in the optimized CPD/$MAPbI_3$/Pt hybrid system, representing the state-of-the-art performance for MHP photocatalysts. This work highlights the excellent charge-transfer ability of CPDs. Moreover, the bandedge-tunable property makes CPDs promising candidates as co-catalysts to match with different-energy-alignment MHPs, indicating their great potential in developing efficient perovskite-based hybrid photocatalysts.

Introduction

Beyond photoelectronic devices,[1–7] metal halide perovskites (MHP) have recently caught increasing attention in photocatalysis because of their wide high absorption coefficients, low surface recombination velocities and easily tunable energy levels.[8–13] In addition to outstanding performance, the impressively labile perovskites exhibit unexpected photocatalytic stability,[14–17] indicating bright prospects of MHP photocatalysts. Typical photocatalytic processes consist of light harvesting, charge transfer and surface reaction.[18–22] Compared to ultrafast light absorption (10^{-12}–10^{-9} s) and fast charge transfer (10^{-9}–10^{-6} s), surface reactions are much slower (10^{-6}–10^{0} s). As this time scale mismatch intrinsically limits photocatalytic reaction efficiency, the enhancement of charge separation to increase separated charge lifetime favours improvement in surface reactions and thus efficiency. In 2017, Nam *et al.* discovered that methylammonium lead iodide ($MAPbI_3$) could be stabilized in saturated aqueous hydroiodic acid (HI) solution, and pioneered perovskite photocatalysts on H_2 evolution *via* HI splitting.[23] Since this pioneering work, some groups have devoted efforts to regulating charge-transfer behaviors of perovskites in this photocatalytic model system. Gradient-level-alignment MHPs ($MAPbBr_{3-x}I_x$)[24] or various electron-transfer materials, such as Pt–TiO_2,[10] reduced graphene oxide (rGO),[16] Ni_3C[17] and black phosphorus (BP),[25] have been used to increase charge separation and catalytic efficiencies in $MAPbI_3$. So far, the highest H_2 evolution rate and solar-to-hydrogen (STH)

[a] *State Key Laboratory of Supramolecular Structure and Materials, College of Chemistry, Jilin University, Changchun 130012, China. E-mail: byangchem@jlu.edu.cn*
[b] *Institute of Functional Nano and Soft Materials (FUNSOM), Jiangsu Key Laboratory for Carbon-based Functional Materials and Devices, Soochow University, Suzhou 215123, China. E-mail: zhkang@suda.edu.cn*

† Electronic supplementary information (ESI) available. See DOI: 10.1039/d0mh00955e

‡ Y. Z. and Q. Z. contributed equally to this work.

efficiency based on MHP photocatalysts for HI splitting are 3742 μmol h^{-1} g^{-1} and 1.42%,[15,17] respectively, leaving much room for the further improvement of charge separation and utilization. In photocatalytic H_2 evolution or other reduction reactions, one should develop ideal semiconductors with long-lifetime photoelectrons as well as co-catalysts to extract the photoholes, thus facilitating the reduction reaction instead of charge recombination.

Carbonized polymer dots (CPDs), as an emerging but significant member of the carbon-based nanomaterials family,[26] have a wide range of applications due to their color-tunable emission, high photo-chemical stability, excellent photophysical/chemical properties, low toxicity and facile preparation.[27–30] CPDs are usually prepared through polymerization crosslinking and carbonization of small molecules and/or polymer precursors with multiple polar groups (carboxyl, amino or hydroxyl).[31] The abundance of surface polar groups allows CPDs to easily bind to the surface of ionic lead halide perovskites with charged grain boundaries. Besides, the energy level of CPDs can be easily manipulated by the choice of precursors and reaction conditions.[32,33] Recently, we observed enhanced charge separation and transfer in CPD/TiO_2 photonic crystal hybrid photocatalysts and CPD-modified perovskite solar cells,[34,35] witnessing outstanding charge-transfer ability of CPDs. Therefore, bandedge-tunable CPDs with excellent charge-transfer ability have great potential in developing efficient perovskite-based hybrid photocatalysts.

In this work, we demonstrate that CPDs can act as an efficient charge modulator to stabilize photo-generated carriers in MHPs, and make the first demonstration of efficient perovskite/CPD hybrid photocatalysts for H_2 evolution. We find that the energy level of CPDs prepared from citric acid (CA) and *p*-aminosalicylic acid (PASA) well matches with that of $MAPbI_3$, and show that CA-PASA CPDs can enhance the separation and stabilization of charges in $MAPbI_3$ perovskites through ultrafast hole extraction, resulting in a 35-fold increase in the rate of visible-light-driven photocatalytic splitting of HI compared to that observed for pure $MAPbI_3$. Consequently, one of the highest STH conversion efficiencies of 2.15% is achieved for an optimized Pt/$MAPbI_3$/CA-PASA CPD hybrid. Moreover, the novel strategy of CA-PASA CPD-assisted hole extraction can be universally applied to improve the performance of previously reported electron-manipulated $MAPbI_3$-based photocatalytic systems. This work provides a new and efficient pathway to modulate carrier dynamics in MHP photocatalysts.

Results and discussion

$MAPbI_3$ was hydrothermally synthesized according to a previously described procedure.[23] The $MAPbI_3$ shows extremely strong absorption in the visible and near-infrared regions (400–800 nm, Fig. 1a). The scanning electron microscopy (SEM) image of $MAPbI_3$ powder shows the presence of microcrystals (inset of Fig. 1a, left), while the high-resolution transmission electron microscopy (HR-TEM) image indicates that these $MAPbI_3$ microcrystals have a well-defined structure with a tetragonal lattice parameter of 0.31 nm

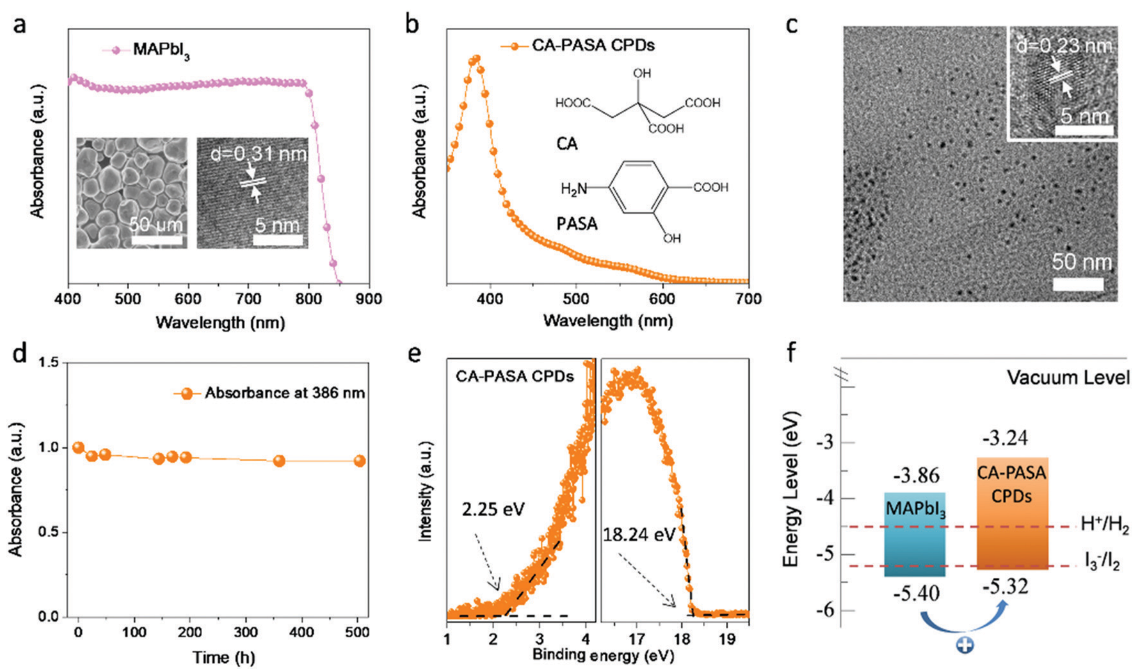

Fig. 1 Characterization of $MAPbI_3$ perovskites and CA-PASA CPDs. (a) Absorption spectrum, SEM and HR-TEM images of $MAPbI_3$. (b) CA-PASA CPD absorption spectrum and their precursor molecular structures. (c) TEM and HR-TEM images of CA-PASA CPDs. (d) Time-dependent absorption intensity of CA-PASA CPDs at 386 nm in HI/H_3PO_2 solution. (e) UPS of CA-PASA CPDs: secondary electron cut-off region (left), magnified spectrum near the Femi edge (right). HOMO = −(21.21–18.24 + 2.25) eV = −5.32 eV. (f) Schematic energy level diagram of $MAPbI_3$ and CA-PASA CPDs and the redox potentials for HI splitting.

along the [220] direction (inset of Fig. 1a, right), which is in good agreement with the corresponding X-ray diffraction pattern (Fig. S1, ESI†).

CA-PASA CPDs were hydrothermally prepared from CA and PASA (inset of Fig. 1b) under acidic conditions (pH 1.0), which were chosen to maximize the carbonization degree and crystallinity and thus improve light harvesting and charge transfer ability.[36] Purified CA-PASA CPDs (Fig. 1b) exhibit strong absorption at 386 nm (with a tail extending to 600 nm) and a bandgap of 2.08 eV (estimated from the related Tauc plot shown in Fig. S2, ESI†). TEM and HR-TEM images show that CA-PASA CPDs are quasi-spherical particles with an average size of 4.9 nm and feature high crystallinity and a lattice pitch of 0.23 nm (Fig. 1c). CA-PASA CPDs exhibit strong fluorescence emission at 507 nm with negligible excitation dependency (Fig. S3, ESI†). Moreover, the stability of CA-PASA CPDs against HI was investigated by recording their time-dependent absorption spectra in HI solution (Fig. 1d and Fig. S4a, ESI†). The almost unchanged absorbance at 386 nm for $>$500 h, as well as intact chemical groups (Fig. S4b, ESI†), indicate that CA-PASA CPDs feature an excellent resistance to acids. Further characterizations illustrate that the multiple polar (carboxyl, amino and hydroxyl) groups of CA and PASA are partially preserved in CA-PASA CPDs (Fig. S4b and c, ESI†). As carboxyl and amino groups are efficient binding sites for stabilizing perovskite nanocrystals,[3,37] the abundance of surface polar groups allows CA-PASA CPDs to easily bind to $MAPbI_3$ perovskites for extracting charge carriers. Therefore, the CA-PASA CPDs/$MAPbI_3$ hybrid can be obtained through self-assembling of CA-PASA CPDs and $MAPbI_3$ in HI solution (Fig. S5a and b, ESI†). Studies on the hybrid catalysts indicate that CA-PASA CPDs bind with $MAPbI_3$ mainly by COO–Pb coordination bond (Fig. S5c–e, ESI†).

Charge separation and transfer efficiencies depend on the alignment of energy levels between $MAPbI_3$ perovskites and CA-PASA CPDs. Ultraviolet photoelectron spectroscopy (UPS) reveals that the CA-PASA CPD highest occupied molecular orbital (HOMO) and lowest unoccupied molecular orbital (LUMO) lie at -5.32 and -3.24 eV, respectively (Fig. 1e). The valence band minimum and conduction band maximum of $MAPbI_3$ perovskites are -5.40 and -3.86 eV, respectively.[38] Thus, staggered energy levels are established between $MAPbI_3$ and CA-PASA CPDs (Fig. 1f). This type-II energy level alignment provides a driving force for hole transfer from $MAPbI_3$ to CA-PASA CPDs, also promoting electron transfer in the opposite direction. Because of the broad and strong absorption of $MAPbI_3$ in hybrid systems, as demonstrated by similar absorption of CPDs/$MAPbI_3$ as pure $MAPbI_3$ (Fig. S6, ESI†), as well as *in situ* transient photovoltage (*in situ* TPV) measurement later. Therefore, the separation of photo-generated charges is concluded to be dominated by hole transfer from $MAPbI_3$ to CA-PASA CPDs, while electron transfer is negligible from the opposite direction.

To study charge transfer between $MAPbI_3$ perovskites and CA-PASA CPDs, we first conducted the steady-state PL and time-resolved PL (TRPL) decay measurements under 450 nm excitation. As shown in Fig. 2a, pure $MAPbI_3$ features a strong interband emission peak at 746 nm, which is indicative of the severe photo-generated charge recombination. However, obvious fluorescence quenching is observed when $MAPbI_3$ was coupled with 1 wt% CA-PASA CPDs. The distinctly suppressed radiative recombination in $MAPbI_3$ suggests the occurrence of charge transfer from $MAPbI_3$ to CA-PASA CPDs,[10] as further demonstrated by TRPL measurements (Fig. 2b). The PL decay plots of $MAPbI_3$ and $MAPbI_3$/CA-PASA CPDs are fitted with a triexponential function (Table S1, ESI†), and the respective average PL lifetimes (56.5 and 35.0 ns) indicate that charge transfer is faster in the hybrid system. Thus, CA-PASA CPDs can effectively extract the holes of $MAPbI_3$ because of the energy level alignment.[10,13]

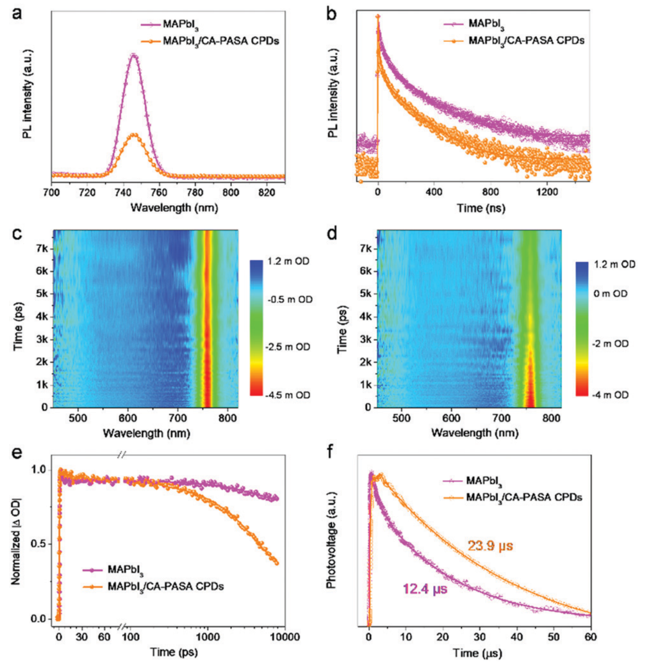

Fig. 2 Enhanced charge separation and lifetime in $MAPbI_3$/CA-PASA CPDs. (a) Steady-state PL and (b) TRPL spectra of $MAPbI_3$ and $MAPbI_3$/CPDs. (c) $MAPbI_3$ and (d) $MAPbI_3$/CPD spectro-temporal TA maps excited at 400 nm. (e) Characteristic dynamics for $MAPbI_3$ and $MAPbI_3$/CPDs probed at 760 nm. (f) TPV curves of $MAPbI_3$ and $MAPbI_3$/CPDs under 355 nm excitation. All hybrid samples contain 1 wt% CPDs.

To gain further insights into ultrafast charge transfer, we investigated the spectral distribution of photo-generated carriers in $MAPbI_3$ and $MAPbI_3$/CA-PASA CPD samples by femtosecond transient absorption (fs-TA) spectroscopy. Two-dimensional fs-TA color maps (Fig. 2c and d) demonstrate an obvious photobleaching (PB) absorption peak at 760 nm for $MAPbI_3$, in good agreement with the previous works.[39] The absence of PB peak redshift indicates a flat energy landscape and negligible adverse bandtail states in the interband,[3] suggesting that $MAPbI_3$ has smooth charge transportation channels and low defect density, and is thus promising for high-performance photocatalytic reactions. After hybridization with CA-PASA CPDs, the fs-TA kinetics at 760 nm become much faster than that of sole $MAPbI_3$ after 231 ps (Fig. 2e), implying that the CA-PASA CPDs can efficiently extract the holes of $MAPbI_3$,[39] consistent with the PL and TRPL results. Given the efficient charge transfer between $MAPbI_3$ and CA-PASA CPDs, the photo-generated carrier lifetime of the $MAPbI_3$/CA-PASA CPD hybrid is expected to be prolonged. To confirm this, we studied the carrier recombination dynamics by transient photovoltage (TPV) measurements, revealing that the half-lifetime of $MAPbI_3$/CA-PASA CPDs (23.9 μs) exceeds that of $MAPbI_3$ (12.4 μs) (Fig. 2f). This charge lifetime increase is ascribed to the enhanced photogenerated charge separation and suppressed recombination in the $MAPbI_3$/CA-PASA CPD hybrid and benefits the surface reaction and, hence, catalytic efficiency.

Based on the above, CA-PASA CPDs are expected to improve the photocatalytic efficiency of $MAPbI_3$ because of their outstanding hole-extraction properties and good stability in HI acid. Previous reports have shown that charge transfer materials can efficiently extract photo-generated carriers through dynamic interaction with perovskites,[10,13] which greatly simplifies the preparation of high-performance perovskite-based hybrid photocatalysts. Therefore, we studied the photocatalytic hydrogen evolution performance of the hybrid prepared by the direct addition of CA-PASA CPDs into the $MAPbI_3$ catalytic system. Photocatalytic reactions were conducted with 100 mg of $MAPbI_3$ in 25 mL of $MAPbI_3$-saturated HI solution under visible light irradiation (λ > 420 nm), and H_2 evolution was monitored by gas chromatograph to probe the influence of CPD content on photocatalytic performance. After 4 h irradiation, 1.33 μmol of H_2 is produced over bare $MAPbI_3$, *i.e.*, the H_2 evolution rate is 3.33 μmol g^{-1} h^{-1} (Fig. 3a and Fig. S7, ESI†). H_2 evolution is significantly enhanced by the introduction of CA-PASA CPDs, with the maximal H_2 evolution rate (115 μmol g^{-1} h^{-1} for $MAPbI_3$/1 wt% CA-PASA CPDs) exceeding that of pure $MAPbI_3$ 35-fold. Only traces of H_2 are detected by gas chromatography when pure CA-PASA CPDs are used as a photocatalyst (Fig. S8, ESI†). Besides, CPD precursors (CA, PASA, and their mixture) have no positive effects on the photocatalytic performance of $MAPbI_3$. All these control experiments indicate that the enhanced performance of $MAPbI_3$/CA-PASA CPDs stems from the synergy between $MAPbI_3$ and CPDs. Moreover, the photocatalytic experiments performed for three types of CPDs with different bandgaps and energy levels highlight the importance of matched energy alignment between CPDs and $MAPbI_3$ (Fig. S9, ESI†). Therefore, the matched energy alignment and high charge transfer capacity of CA-PASA CPDs are concluded to greatly enhance hole extraction and thus improve the performance of $MAPbI_3$-based perovskite photocatalysts.

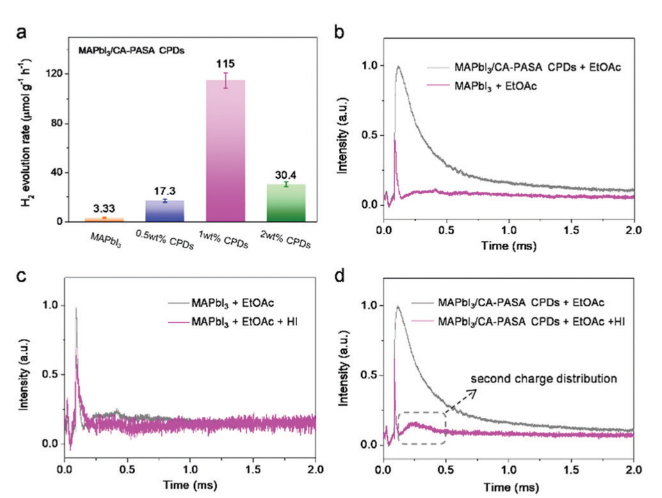

Fig. 3 Photocatalytic performance and mechanism. (a) Rate of H_2 evolution over $MAPbI_3$ hybrids with different CPD contents. (b) *In situ* TPV curves of $MAPbI_3$ and CA-PASA CPDs covered with EtOAc. *In situ* TPV curves recorded with (c) $MAPbI_3$ and (d) CA-PASA CPD/$MAPbI_3$ working electrodes in 1 vol% HI/EtOAc mixed solution (v/v).

The mechanism of the photocatalytic reaction over $MAPbI_3$/CA-PASA CPDs was further probed by *in situ* TPV measurements. The photocatalysts are deposited onto indium-tin oxide (ITO) as working electrodes, with details provided in the ESI.† During testing, the electrodes are covered with a N_2-saturated inactive solvent (ethyl acetate, EtOAc) or reaction solution (1% HI/EtOAc, v/v), which allows one to directly observe the surface reactions of photo-generated charges. We first investigated the effects of CA-PASA CPDs on the photocurrent signals of $MAPbI_3$ with no charge consumer (HI). As shown in Fig. 3b, the photocurrent intensity of $MAPbI_3$/CA-PASA CPDs is much higher than that of $MAPbI_3$, indicating a larger photo-generated charge concentration on the surface of the former and a higher electron–hole separation efficiency. Besides, the delayed attenuation of $MAPbI_3$/CA-PASA CPDs suggests longer photo-generated charge lifetime. This observation is consistent with the conclusion that CA-PASA CPDs can enhance the charge separation and lifetime of $MAPbI_3$ in the study of ultrafast photophysical processes (Fig. 2). Subsequently, the process of photocatalytic HI splitting was explored. For $MAPbI_3$ as the working electrode (Fig. 3c), the photocurrent intensity decreases under 1% HI/EtOAc conditions, indicating that the photo-generated charges of $MAPbI_3$ are consumed to split HI. When CA-PASA CPDs are introduced (Fig. 3d), the photocurrent of $MAPbI_3$/CA-PASA CPDs in 1% HI/EtOAc presents a much sharper decay than that of $MAPbI_3$, which implies a faster charge transfer from $MAPbI_3$/CA-PASA CPDs to the catalyst/reactant interface. In addition, after the initial fast consumption of charges by HI, a broad shoulder peak at 0.2–0.5 ms appears again, which corresponds to the second distribution of photo-generated charges between the catalyst/solution interface. However, no second charge distribution is observed during HI splitting over pure $MAPbI_3$ (Fig. 3c). Therefore, CA-PASA CPDs are concluded to induce a second charge migration from the interior of $MAPbI_3$ to the catalyst/reactant interface, which increases the reaction efficiency of photo-generated charges. This phenomenon is ascribed to the excellent charge extraction and stabilization ability of CA-PASA CPDs.

Given the poor light response of CA-PASA CPDs (Fig. S10, ESI†), electrons and holes are concluded to be primarily generated from $MAPbI_3$. These *in situ* TPV results confirm that $MAPbI_3$ is the main photoactive component in this hybrid system, while CA-PASA CPDs are a superb charge transfer medium to stabilize photogenerated charges and increase their lifetime. The separated charges in $MAPbI_3$/CA-PASA CPDs show a fast

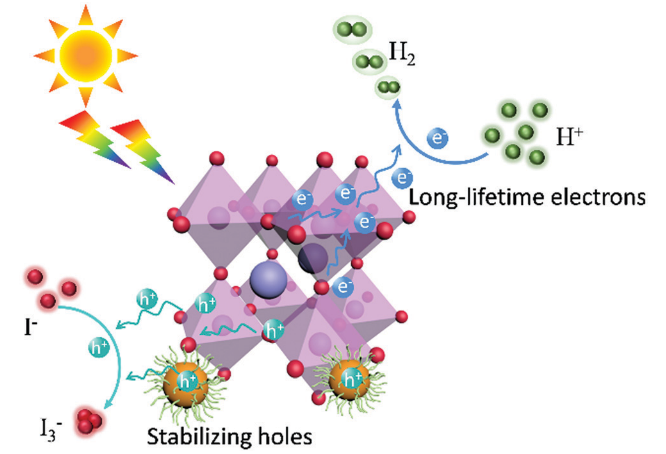

Scheme 1 Schematic diagram of the photocatalytic mechanism for CA-PASA CPDs/$MAPbI_3$.

surface reaction rate and improved catalytic efficiency. The mechanism of catalytic HI splitting over $MAPbI_3$/CA-PASA CPDs is provided in Scheme 1. When light strikes on the hybrid photocatalyts, $MAPbI_3$ absorbs light energy to produce electrons and holes. Driven by the staggered energy alignment, CA-PASA CPDs extract holes and enhance charge separation to increase the lifetime of electrons in $MAPbI_3$ and thus promote photocatalytic H_2 evolution.

In $MAPbI_3$/CPD photocatalysts, the long-lifetime photo-generated electrons in $MAPbI_3$ reduce H^+ to produce H_2. Theoretical calculations indicate that both the MA^+ and Pb^{2+} cations of $MAPbI_3$ participate in reduction processes and act as active sites to produce H_2 *via* a two-step reaction.[40] As H^+ reduction on the perovskite surface is slow, we attempted to accelerate it by loading a Pt co-catalyst to further improve the catalytic efficiency of $MAPbI_3$/CA-PASA CPDs.[23,24] As shown in Fig. 4a, the H_2 evolution rate of $MAPbI_3$/1 wt% CA-PASA CPDs increases to 6594 μmol g^{-1} h^{-1} after the loading of 0.75 wt% Pt. Control experiments show that $MAPbI_3$/Pt present a low H_2 evolution rate of 25.4 μmol g^{-1} h^{-1}, while the activity of CPDs/Pt is close to zero (Fig. S11, ESI†). These results suggest that the outstanding performance of Pt/$MAPbI_3$/CA-PASA CPDs stems from the seamless cooperation between all constituents. The excellent ability of CA-PASA CPDs to extract holes from $MAPbI_3$ promotes charge separation and prolongs the lifetime of photo-generated charges at the $MAPbI_3$/CA-PASA CPD interface. Once Pt is loaded, the active sites of H_2 reduction shift from $MAPbI_3$ to Pt, which features a much higher H_2 evolution activity, and the photo-generated electrons can be rapidly consumed. Therefore, one expects that photocatalytic efficiency can be appreciably improved by further enhancement of dynamic charge extraction and separation between $MAPbI_3$ and CA-PASA CPDs through increasing the amount of CPDs. The H_2 evolution rate of Pt/$MAPbI_3$/7 wt% CPDs equals 11 497 μmol g^{-1} h^{-1}, and the corresponding STH conversion efficiency reaches 2.15%. Both of these values are among the highest reported for MHP-based photocatalysts (Fig. 4b and Table S2, ESI†). The above optimal photocatalyst presents a high apparent quantum yield (AQY) of

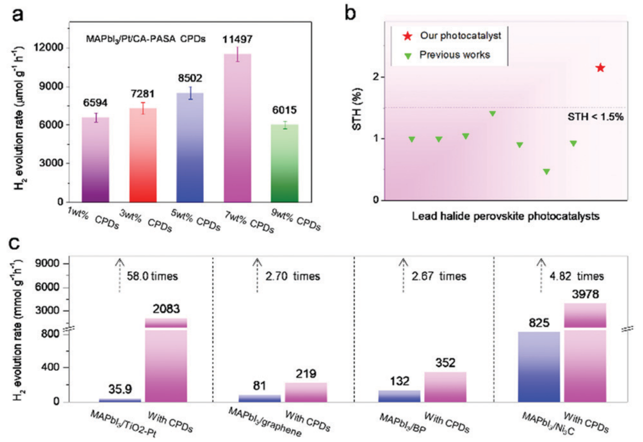

Fig. 4 Efficiency optimization and performance comparison of CA-PASA CPDs with other electron-transfer materials. (a) Rate of H_2 evolution on Pt/$MAPbI_3$/CA-PASA CPDs with different CPD contents. (b) STH conversion efficiencies of previous MHP photocatalysts.[10,13,15–17,23–25,37,38,41–44] (c) Rate of H_2 evolution on $MAPbI_3$/TiO_2–Pt, $MAPbI_3$/graphene, $MAPbI_3$/BP, $MAPbI_3$/Ni_3C, and their CA-PASA CPD-hybrid systems.

53.6% at 420 nm and shows good performance and structure stability during three reaction cycles (Fig. S13, ESI†).

The above discussion indicates that hole extraction by CA-PASA CPDs is a novel and efficient method of enhancing charge separation and improving the lifetime of photo-generated electrons in the $MAPbI_3$ perovskite. Therefore, this performance improvement strategy should be applicable to previously reported electron-manipulated $MAPbI_3$ hybrid systems. To test this hypothesis, we prepared typical $MAPbI_3$-based hybrid photocatalysts with four different electron-transfer materials, namely TiO_2–Pt,[10] graphene,[16] black phosphorus (BP),[25] and Ni_3C[17] (Fig. S14, ESI†), which were loaded at optimal contents determined in previous works. As shown in Fig. 4c, the above systems show higher H_2 evolution rates than sole $MAPbI_3$ (3.33 μmol g^{-1} h^{-1}), consistent with the previous works. As expected, coupling with CA-PASA CPDs (Fig. 4c and Fig. S15, ESI†) improves the performance of all systems (by factors of 58.0, 2.70, 2.67, and 4.82 for $MAPbI_3$/TiO_2–Pt, $MAPbI_3$/graphene, $MAPbI_3$/BP, and $MAPbI_3$/Ni_3C, respectively). These results indicate that CA-PASA CPDs have a universally positive impact on electron-manipulated $MAPbI_3$ photocatalytic systems.

Conclusions

In summary, we demonstrate that CPDs can act as an efficient charge modulator to stabilize photo-generated carriers in MHPs. The CA-PASA CPDs can efficiently enhance the charge separation and lifetime of $MAPbI_3$ perovskite through ultra-fast hole transfer, thus leading to a 35-fold increase in the rate of visible-light-driven photocatalytic HI splitting. The optimal Pt/$MAPbI_3$/CPD hybrid system exhibits a high H_2 evolution rate of 11 497 μmol h^{-1} g^{-1} and a record STH efficiency of 2.15%. Furthermore, CA-PASA CPDs can universally promote the performance of previous electron-manipulated $MAPbI_3$-based photocatalysts. The bandedge-tunable property makes CPDs ideal candidates as co-catalysts to match with various MHP photocatalysts with different energy alignments. This work highlights the excellent charge-transfer ability of CPDs and their great potential in developing efficient perovskite-based hybrid photocatalysts.

Author contributions

B. Y. supervised the whole project. Y. Z., Q. Z. and B. Y. conceived the experiments. Y. Z. and Q. Z. contributed to all the experimental work. T. F., C. L. and J. L contributed to the synthesis and characterization of CPDs and perovskite. Y. Y. and Z. W. assisted the photocatalytic test. Y. Z., Y. L. and Z. K. carried out the *in situ* TPV and analysed the results. H. W. S. Z. and H. Z. helped to analyse the experimental results and modify English. Y. Z., Q. Z. and B. Y. wrote the manuscript. All the authors commented on the paper.

Conflicts of interest

The authors declare no conflicts of interest.

Acknowledgements

This work was financially supported by the National Science Foundation of China (NSFC) under Grant No. 51433003, the National Basic Research Program of China (973 Program) under Grant No. 2014CB643503, the China Postdoctoral Science Foundation under Grant No. 2019M661202, the Opening Funds of State Key Laboratory of Applied Optics, Changchun Institute of Optics, Fine Mechanics and Physics, Chinese Academy of Science, and the JLU Science and Technology Innovative Research Team 2017TD-06.

References

1 J. P. Correa-Baena, M. Saliba, T. Buonassisi, M. Gratzel, A. Abate, W. Tress and A. Hagfeldt, *Science*, 2017, **358**, 739–744.
2 H. Wei, Y. Fang, P. Mulligan, W. Chuirazzi, H.-H. Fang, C. Wang, B. R. Ecker, Y. Gao, M. A. Loi, L. Cao and J. Huang, *Nat. Photonics*, 2016, **10**, 333–339.
3 Q. Zeng, X. Zhang, X. Feng, S. Lu, Z. Chen, X. Yong, S. A. T. Redfern, H. Wei, H. Wang, H. Shen, W. Zhang, W. Zheng, H. Zhang, J. S. Tse and B. Yang, *Adv. Mater.*, 2018, **30**, 1705393.
4 W. Zhu, W. Ma, Y. Su, Z. Chen, X. Chen, Y. Ma, L. Bai, W. Xiao, T. Liu, H. Zhu, X. Liu, H. Liu, X. Liu and Y. M. Yang, *Light: Sci. Appl.*, 2020, **9**, 112.
5 H. Sun, Z. Yang, M. Wei, W. Sun, X. Li, S. Ye, Y. Zhao, H. Tan, E. L. Kynaston, T. B. Schon, H. Yan, Z. H. Lu, G. A. Ozin, E. H. Sargent and D. S. Seferos, *Adv. Mater.*, 2017, **29**, 1701153.
6 J. Xing, C. Zhao, Y. Zou, W. Kong, Z. Yu, Y. Shan, Q. Dong, D. Zhou, W. Yu and C. Guo, *Light: Sci. Appl.*, 2020, **9**, 111.
7 Q. Zeng, X. Zhang, C. Liu, T. Feng, Z. Chen, W. Zhang, W. Zheng, H. Zhang and B. Yang, *Sol. RRL*, 2019, **3**, 1800239.
8 M. Ou, W. Tu, S. Yin, W. Xing, S. Wu, H. Wang, S. Wan, Q. Zhong and R. Xu, *Angew. Chem.*, 2018, **130**, 13758–13762.
9 J. Chen, C. Dong, H. Idriss, O. F. Mohammed and O. M. Bakr, *Adv. Energy Mater.*, 2020, **10**, 1902433.
10 X. Wang, H. Wang, H. Zhang, W. Yu, X. Wang, Y. Zhao, X. Zong and C. Li, *ACS Energy Lett.*, 2018, **3**, 1159–1164.
11 D. Yue, T. Zhang, T. Wang, X. Yan, C. Guo, X. Qian and Y. Zhao, *EcoMat*, 2020, **2**, e12015.
12 Y. Zhao, T. Wang, T. Zhang and X. Li, *Acta Chim. Sin.*, 2019, **77**, 1075.
13 H. Wang, X. Wang, R. Chen, H. Zhang, X. Wang, J. Wang, J. Zhang, L. Mu, K. Wu, F. Fan, X. Zong and C. Li, *ACS Energy Lett.*, 2018, **4**, 40–47.
14 X. Zhu, Y. Lin, J. San Martin, Y. Sun, D. Zhu and Y. Yan, *Nat. Commun.*, 2019, **10**, 2843.
15 Z. Zhao, J. Wu, Y.-Z. Zheng, N. Li, X. Li, Z. Ye, S. Lu, X. Tao and C. Chen, *Appl. Catal., B*, 2019, **253**, 41–48.
16 Y. Wu, P. Wang, X. Zhu, Q. Zhang, Z. Wang, Y. Liu, G. Zou, Y. Dai, M. H. Whangbo and B. Huang, *Adv. Mater.*, 2018, **30**, 1704342.
17 Z. Zhao, J. Wu, Y.-Z. Zheng, N. Li, X. Li and X. Tao, *ACS Catal.*, 2019, **9**, 8144–8152.
18 Z. Wang and L. Wang, *Chin. J. Catal.*, 2018, **39**, 369–378.
19 S. J. Phang and L.-L. Tan, *Catal. Sci. Technol.*, 2019, **9**, 5882–5905.
20 X. C. Ma, Y. Dai, L. Yu and B. B. Huang, *Light: Sci. Appl.*, 2016, **5**, e16017.
21 Y. Wang, Y. Wu, K. Sun and Z. Mi, *Mater. Horiz.*, 2019, **6**, 1454–1462.
22 F. Pincella, K. Isozaki and K. Miki, *Light: Sci. Appl.*, 2014, **3**, e133.
23 S. Park, W. J. Chang, C. W. Lee, S. Park, H.-Y. Ahn and K. T. Nam, *Nat. Energy*, 2017, **2**, 16185.
24 Y. Wu, P. Wang, Z. Guan, J. Liu, Z. Wang, Z. Zheng, S. Jin, Y. Dai, M.-H. Whangbo and B. Huang, *ACS Catal.*, 2018, **8**, 10349–10357.
25 R. Li, X. Li, J. Wu, X. Lv, Y.-Z. Zheng, Z. Zhao, X. Ding, X. Tao and J.-F. Chen, *Appl. Catal., B*, 2019, **259**, 118075.
26 S. Tao, T. Feng, C. Zheng, S. Zhu and B. Yang, *J. Phys. Chem. Lett.*, 2019, **10**, 5182–5188.
27 D. Li, D. Han, S. N. Qu, L. Liu, P. T. Jing, D. Zhou, W. Y. Ji, X. Y. Wang, T. F. Zhang and D. Z. Shen, *Light: Sci. Appl.*, 2016, **5**, e16120.
28 B. Wang, J. Li, Z. Tang, B. Yang and S. Lu, *Sci. Bull.*, 2019, **64**, 1285–1292.
29 Y. Liu, X. Li, Q. Zhang, W. Li, Y. Xie, H. Liu, L. Shang, Z. Liu, Z. Chen, L. Gu, Z. Tang, T. Zhang and S. Lu, *Angew. Chem., Int. Ed.*, 2020, **59**, 1718–1726.
30 X. Bao, Y. Yuan, J. Chen, B. Zhang, D. Li, D. Zhou, P. Jing, G. Xu, Y. Wang, K. Hola, D. Shen, C. Wu, L. Song, C. Liu, R. Zboril and S. Qu, *Light: Sci. Appl.*, 2018, **7**, 91.
31 D. Qu and Z. Sun, *Mater. Chem. Front.*, 2020, **4**, 400–420.

32 T. Ji, B. Guo, F. Liu, Q. Zeng, C. Yu, X. Du, G. Jin, T. Feng, S. Zhu, F. Li and B. Yang, *Adv. Mater. Interfaces*, 2018, **5**, 1701519.
33 J. Liu, D. Li, K. Zhang, M. Yang, H. Sun and B. Yang, *Small*, 2018, **14**, e1703919.
34 X. Zhang, Q. Zeng, Y. Xiong, T. Ji, C. Wang, X. Shen, M. Lu, H. Wang, S. Wen, Y. Zhang, X. Yang, X. Ge, W. Zhang, A. P. Litvin, A. V. Baranov, D. Yao, H. Zhang, B. Yang, A. L. Rogach and W. Zheng, *Adv. Funct. Mater.*, 2020, **30**, 1910530.
35 Y. Zhao, Q. Zeng, T. Feng, C. Xia, C. Liu, F. Yang, K. Zhang and B. Yang, *Mater. Chem. Front.*, 2019, **3**, 2659–2667.
36 T. Feng, Q. Zeng, S. Lu, X. Yan, J. Liu, S. Tao, M. Yang and B. Yang, *ACS Photonics*, 2017, **5**, 502–510.
37 M. Xiao, M. Hao, M. Lyu, E. G. Moore, C. Zhang, B. Luo, J. Hou, J. Lipton-Duffin and L. Wang, *Adv. Funct. Mater.*, 2019, **29**, 1905683.
38 M. Wang, Y. Zuo, J. Wang, Y. Wang, X. Shen, B. Qiu, L. Cai, F. Zhou, S. P. Lau and Y. Chai, *Adv. Energy Mater.*, 2019, **9**, 1901801.
39 Z. Zhu, J. Ma, Z. Wang, C. Mu, Z. Fan, L. Du, Y. Bai, L. Fan, H. Yan, D. L. Phillips and S. Yang, *J. Am. Chem. Soc.*, 2014, **136**, 3760–3763.
40 L. Wang, H. Xiao, T. Cheng, Y. Li and W. A. Goddard 3rd, *J. Am. Chem. Soc.*, 2018, **140**, 1994–1997.
41 Z. Guan, Y. Wu, P. Wang, Q. Zhang, Z. Wang, Z. Zheng, Y. Liu, Y. Dai, M.-H. Whangbo and B. Huang, *Appl. Catal., B*, 2019, **245**, 522–527.
42 Y. Guo, G. Liu, Z. Li, Y. Lou, J. Chen and Y. Zhao, *ACS Sustainable Chem. Eng.*, 2019, **7**, 15080–15085.
43 T. Wang, D. Yue, X. Li and Y. Zhao, *Appl. Catal., B*, 2020, **268**, 118399.
44 H. Zhao, Y. Li, B. Zhang, T. Xu and C. Wang, *Nano Energy*, 2018, **50**, 665–674.